ACS chemical biology

Articles

pubs.acs.org/acschemicalbiology

Understanding Dengue Virus Capsid Protein Disordered N-Terminus and pep14-23-Based Inhibition

André F. Faustino,[†] Gabriela M. Guerra,[†] Roland G. Huber,[‡] Axel Hollmann,[†] Marco M. Domingues,[†] Glauce M. Barbosa,[§] Francisco J. Enguita,[†] Peter J. Bond,[‡,∥] Miguel A. R. B. Castanho,[†] Andrea T. Da Poian,[§] Fabio C. L. Almeida,[§,⊥] Nuno C. Santos,*[,†] and Ivo C. Martins*[,†]

[†]Instituto de Medicina Molecular, Faculdade de Medicina, Universidade de Lisboa, Av. Prof. Egas Moniz, 1649-028 Lisbon, Portugal

[‡]Bioinformatics Institute (BII), Agency for Science, Technology and Research (A*STAR), 30 Biopolis Street, #07-01 Matrix, 138671 Singapore, Singapore

[§]Instituto de Bioquímica Médica Leopoldo de Meis, Universidade Federal do Rio de Janeiro, Rio de Janeiro, RJ 21941-902, Brazil

[∥]Department of Biological Sciences, National University of Singapore, 14 Science Drive 4, 117543 Singapore, Singapore

[⊥]Centro Nacional de Ressonância Magnética Nuclear, Universidade Federal do Rio de Janeiro and National Institute of Structural Biology and Bioimage, Rio de Janeiro, RJ 21941-902, Brazil

Supporting Information

ABSTRACT: Dengue virus (DENV) infection affects millions of people and is becoming a major global disease for which there is no specific available treatment. pep14-23 is a recently designed peptide, based on a conserved segment of DENV capsid (C) protein. It inhibits the interaction of DENV C with host intracellular lipid droplets (LDs), which is crucial for viral replication. Combining bioinformatics and biophysics, here, we analyzed pep14-23 structure and ability to bind different phospholipids, relating that information with the full-length DENV C. We show that pep14-23 acquires α-helical conformation upon binding to negatively charged phospholipid membranes, displaying an asymmetric charge distribution structural arrangement. Structure prediction for the N-terminal segment reveals four viable homodimer orientations that alternatively shield or expose the DENV C hydrophobic pocket. Taken together, these findings suggest a new biological role for the disordered N-terminal region, which may function as an autoinhibitory domain mediating DENV C interaction with its biological targets. The results fit with our current understanding of DENV C and pep14-23 structure and function, paving the way for similar approaches to understanding disordered proteins and improved peptidomimetics drug development strategies against DENV and similar *Flavivirus* infections.

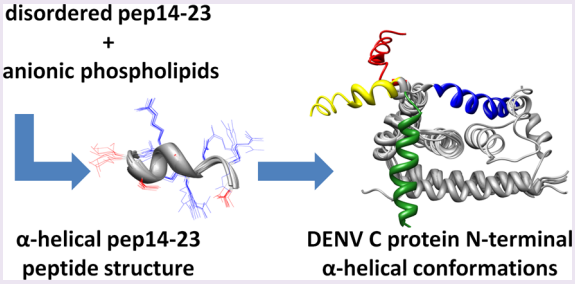

Dengue virus (DENV) causes a mosquito-borne disease that affects around 390 million people worldwide, originating over half a million hospitalizations and 20 000 deaths every year.[1,2] DENV is a member of the *Flavivirus* genus of the *Flaviviridae* family, a taxon comprising several other major human pathogens, such as the yellow fever virus, West Nile virus, tick-borne encephalitis virus, and hepatitis C virus.[3,4] DENV is transmitted between humans via the bite of *Aedes aegypti* or *Aedes albopictus* female mosquitoes.[5] Globalization of trade and travel, besides increasing the virus distribution area, also prompts the spread of the vector worldwide, together with climate change.[2,5] *Aedes spp.* mosquitoes reach now temperate regions, including North America and Europe.[6−8] This resulted in recent autochthonous DENV transmission in France, Croatia, and Portugal (Madeira island), demonstrating the disease global reach.[9−11]

Dengue is the world's fastest-growing tropical disease for which there are no effective and specific treatments or commercial vaccines,[2,12] partially due to the lack of knowledge on basic aspects of the viral life cycle.[13] The virus is relatively simple: it possesses only ten proteins, of which three are structural and seven nonstructural proteins (for a review, see refs 13 and 14). Of particular interest, as drug targets are the structural proteins, namely, the capsid (C) protein, given the variety of functions in which it is involved. Flaviviruses C proteins have a clear structural function in the mature virion, while also performing essential roles in the viral assembly and encapsidation processes.[15−17] Importantly, the interaction of DENV C with host lipid droplets (LDs; intracellular deposits of lipids associated with specific proteins) is required for successful viral replication.[16] Furthermore, drugs impairing LDs biogenesis significantly inhibit viral production at the particle assembly step of the replication cycle.[16]

Received: August 13, 2014
Accepted: November 3, 2014

   dx.doi.org/10.1021/cb500640t | *ACS Chem. Biol.* XXXX, XXX, XXX−XXX

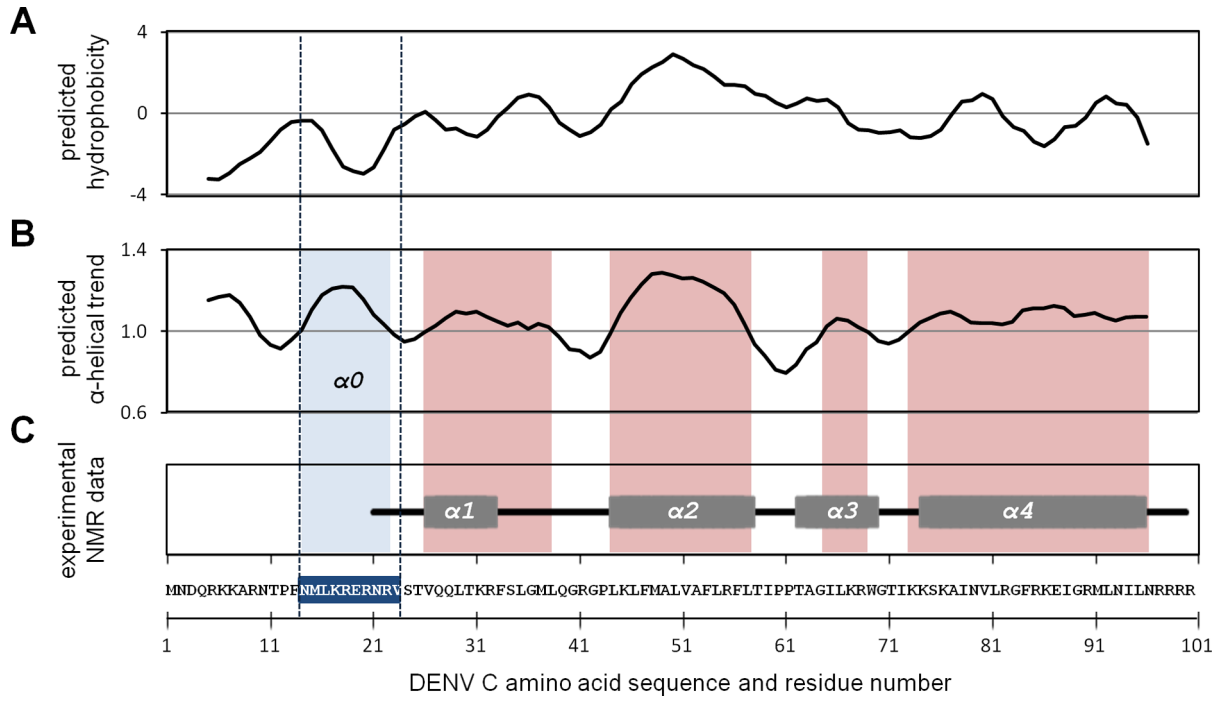

Figure 1. Predicted hydrophobicity and α-helical propensity compared to the experimental DENV C structure. (A) Predicted hydrophobicity and (B) α-helical structure propensity (red shadowed areas) were determined for DENV C sequence and compared to (C) the experimentally determined secondary structure of DENV C residues 21 to 100 (PDB ID: 1R6R,[23] residues 1 to 20 have not been assigned to any experimental structure), where gray bars correspond to α-helical domains (α1, α2, α3, and α4) and black lines stand for residues within loops. The blue shadowed area limited shows an amphipathic behavior with a tendency toward forming an α-helical structure, here named α0. The section within dashed lines corresponds to the region similar to pep14-23.

We recently characterized DENV C interaction with LDs.[18,19] This interaction was found to be strong and dependent on the high intracellular potassium concentration.[18] Limited proteolysis of LDs and atomic force microscopy experiments show that DENV C-LDs interaction require LDs surface proteins and that perilipin 3, also known as TIP47, is the major protein ligand of DENV C on the LDs surface.[18] DENV C-LDs binding was found to require a conserved segment of the DENV C N-terminal region, which led to the design of pep14-23.[19,20] pep14-23 is a 10 amino acid residues peptide based on a consensus motif between DENV C and mosquito-borne flaviviruses C proteins (DENV C residues 14 to 23). This conserved motif contains residues functionally relevant for DENV C interaction with LDs. pep14-23 therefore partially corresponds to DENV C intrinsically disordered N-terminal region (residues 1 to 26). This peptide binds LDs and successfully inhibits DENV C-LDs interaction.[19] DENV C interaction with plasma lipoproteins was also studied. DENV C interacts specifically with very low-density lipoproteins (but not with low-density lipoproteins), which may allow the formation of highly infectious lipoviroparticles.[21] Interestingly, DENV C binding to very low-density lipoproteins also requires K^+, may involve structurally similar proteins, and is also inhibited by pep14-23.[18−22]

The pep14-23 peptide and the N-terminal region of DENV C in which it is based are thus extremely relevant for drug design and deserve further study. Here, we found that pep14-23 binds to anionic phospholipids, acquiring α-helical conformation. We then established its tridimensional structure via nuclear magnetic resonance (NMR) spectroscopy. Following, we evaluated these data in the context of the possible protein structures for DENV C N-terminus and analogous sequences in similar autoinhibitory proteins. The results show that pep14-23 and the corresponding section of the DENV C N-terminal may acquire α-helical conformations that can inhibit the hydrophobic core of the C protein from interacting with lipid systems, suggesting future improved inhibition strategies.

RESULTS AND DISCUSSION

DENV C N-Terminal Region May Become α-Helical. An *in silico* analysis of DENV C hydrophobicity (Figure 1A) and α-helical secondary structure (Figure 1B) propensity was performed in the context of the secondary structure experimental information available (Figure 1C, previously determined by NMR[23]). In Figure 1A, negative local minima indicate hydrophilic regions, while positive local maxima suggest hydrophobic regions. The predicted hydrophobicity data match with the experimental information.[23] The most hydrophobic region corresponds to residues 44 to 66, which includes α-helix 2 and are part of a conserved central hydrophobic pocket. The α-helix 4, an heavily charged C-terminal section, is not predicted to be hydrophobic, as expected. The regions corresponding to α-helices α1, α3, and α4, and intermediate loops display an hydrophobicity around 0, indicating amphiphilic regions. Regarding the N-terminal region, a more complex picture emerges. The first N-terminal residues are charged and possess little affinity toward hydrophobic systems. However, the residues that correspond to pep14-23 (blue shadowed in Figure 1) show an oscillation in the hydrophobicity profile, with a maximum value close to −0.3 at Asn14 and a minimum close to −3 at Arg20. Essentially, the first half of the pep14-23 homologous sequence is mostly hydrophobic, while the second half is more polar. Given this amphipathic nature, it may interact with lipid systems. Since

dx.doi.org/10.1021/cb500640t | ACS Chem. Biol. XXXX, XXX, XXX−XXX

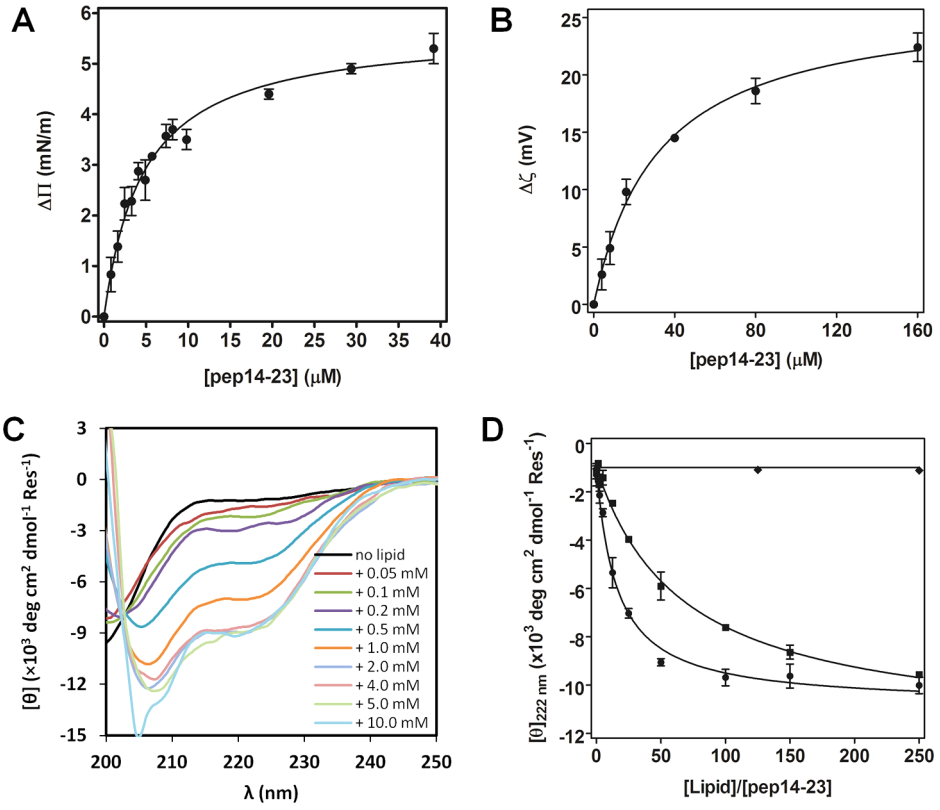

Figure 2. pep14-23 interacts with anionic phospholipids acquiring α-helical structure. (A) Tensiometry analysis of POPG monolayers with the addition of increasing pep14 23 concentrations in buffer containing Na^+. (B) Zeta potential analysis of POPG LUV (bilayers) at 200 μM in buffer containing Na^+ ions with different pep14-23 concentration. (C) CD spectra of pep14-23 at 40 μM in the presence of different concentrations of POPG LUV. (D) Comparison of the pep14-23 $[\theta]$ signal at 222 nm (a local minima for α-helices) at different lipid-to-peptide molar ratios, for LUV with three different lipid compositions (all prepared in buffer containing Na^+): POPG (●), POPG:POPC 1:1 molar ratio (■), and POPC (♦). Solid lines represent fits to the experimental data. Experiments were conducted in triplicate and data are represented as mean ± SD. Fitting equations and calculated parameters are presented in Table 1. See also Supporting Information Table S1 and Figures S1 and S2.

peptide secondary structure can be significantly affected by lipid membranes (reviewed elsewhere[24,25]), the α-helix propensity of the full-length 100 amino acids DENV C protein was also studied (Figure 1B) and compared with the section of DENV C for which there is experimental structural information (residues 21 to 100, Figure 1C). Regions where α-helix conformation was experimentally observed[23,26] are predicted to possess α-helical structure (values higher than 1; red shadowed areas of Figure 1), showing good agreement between theoretical and experimental data. Regarding the N-terminal region of DENV C for which there are no experimental data available, the predictions show that it also may acquire α-helical structure, especially in the region corresponding to residues 14 to 22, which we labeled as a hypothetical α-helical region "α0" (Figure 1B; blue shadowed column). This theoretical helical region is conserved in other mosquito-borne flaviviruses' capsid proteins[19] and practically superimposes with pep14-23 sequence. pep14-23 may therefore be able to interact with lipids and acquire an α-helical conformation. This hypothesis was directly tested by studying pep14-23.

Anionic Phospholipids Convert pep14-23 to α-Helix. The ability of pep14-23 to interact with phospholipids was evaluated both with 1-palmitoyl-2-oleoyl-*sn*-glycero-3-phosphocholine (POPC; zwitterionic) and 1-palmitoyl-2-oleoyl-*sn*-glycero-3-phospho-(1′-*rac*-glycerol) (POPG; negative net charge). Peptide binding to POPG monolayers and bilayers was analyzed by tensiometry and zeta potential (Figure 2A and B, respectively). In our study, tensiometry was used to measure the variation of the surface pressure ($\Delta\Pi$) of phospholipid monolayers caused by the interaction (or insertion) of the peptide. Zeta potential was employed to measure the surface charge density distribution changes. Both $\Delta\Pi$ and zeta potential show that pep14-23 interacts with POPG-containing lipid systems (Figure 2A and B). Measurements show a continuous $\Delta\Pi$ increase upon the addition of pep14-23, reaching a maximal surface pressure variation of 5.67 ± 0.14 mN m^{-1}. Zeta potential analyses show the same: in the absence of the peptide, POPG vesicles present a zeta potential of −43.7 ± 1.5 mV. Peptide addition to the lipid vesicles increases the zeta potential toward positive values up to −21.3 ± 1.1 mV at the highest pep14-23 concentration tested. No interaction was observed with zwitterionic POPC vesicles (not shown).

Having established that the peptide binds to negatively charged phospholipid monolayers and bilayers, and given that DENV C N-terminal region shows a tendency to form α-helix (Figure 1B; "α0", residues 14 to 22), we evaluated by circular dichroism spectroscopy (CD) pep14-23 peptide secondary structure in aqueous and membrane environments (Figure 2C and Supporting Information Figure S1). First, we tested the effect of phospholipids composition at a fixed large unilamelar vesicles (LUV) concentration (Supporting Information Figure S1A). CD spectra of pep14-23 were obtained at 0.5 mM lipid concentration using vesicles composed of POPC only, POPG only, and different POPC:POPG molar ratios (4:1, 3:2, and

dx.doi.org/10.1021/cb500640t | ACS Chem. Biol. XXXX, XXX, XXX−XXX

Table 1. Fit Equations, Parameters and Statistical Comparison of pep14-23 Interaction with POPG Monolayers and Bilayers (LUV) in Na^+ and K^+ Buffers[a]

technique	fitting equation	parameter	Na^+ buffer	K^+ buffer	p
tensiometry	$\Delta\Pi = \frac{\Delta\Pi_{max}[P]}{K_D^{app} + [P]}$	$\Delta\Pi_{max}$ (mN m^{-1})	5.67 ± 0.14	4.55 ± 0.12	<0.0001
		K_D^{app} (μM)	4.63 ± 0.34	4.84 ± 0.45	0.76
zeta potential	$\Delta\zeta = \frac{\Delta\zeta_{max}[P]}{K_D^{app} + [P]}$	$\Delta\zeta_{max}$ (mV)	26.5 ± 0.95	27.4 ± 1.34	0.58
		K_D^{app} (μM)	31.9 ± 3.3	33.5 ± 4.9	0.78
circular dichroism	$\Delta[\theta] = \frac{\Delta[\theta]_{max}[L]}{K_D^{app} + [L]}$	$\Delta[\theta]_{max}$ ($\times 10^3$ deg cm^2 $dmol^{-1}$ Res^{-1})	−9.83 ± 0.22	−9.60 ± 0.21	0.44
		K_D^{app} (μM)	627 ± 59	527 ± 48	0.17

[a]Following previous approaches,[18,27,28] the data were fitted using the equations displayed below. The half-maximal effect (K_D^{app}) represents an apparent binding constant (not directly comparable between techniques). Values are presented as mean ± SEM. See also Figure 2.

1:1). It was observed that the most negatively charged pure POPG vesicles induce a small α-helical conformational switch at that concentration. To confirm the importance of lipid composition, we assessed the effect of zwitterionic POPC vesicles (neutral net charge). It was clear that, even at high concentrations, pure POPC vesicles do no trigger a conformational change on pep14-23 (Supporting Information Figure S1B). To further test the effect of negative lipid vesicles, we evaluated POPC:POPG vesicles at a 1:1 molar ratio (Supporting Information Figure S1C). POPC:POPG 1:1 vesicles clearly induce a conformational conversion of pep14-23 to α-helix, especially at high total lipid concentrations (Supporting Information Figure S1C). This phospholipid negative charge effect is further confirmed and more pronounced when vesicles composed only of the negatively charged POPG are employed (Figure 2C). Not only a similar switch of pep14-23 from random coil to α-helix is observed with pure POPG vesicles but that also occurs at lower lipid concentrations (Figure 2C). In Figure 2D, we integrate this structural information by plotting the ellipticity signal ($[\theta]$) at 222 nm (one of the minima of the α-helix, where any noise that may occur at the lower wavelengths for the highest lipid concentrations is also avoided) as a function of the lipid-to-peptide molar ratio, for different membrane compositions. The effect of negatively charged lipids on pep14-23 conversion to α-helix is clear (Figure 2D). The corresponding parameters for the fitted curves displayed in Figure 2D are detailed in Supporting Information Table S1. The half-maximal effects for the pep14-23 α-helical conversion in POPG and POPC:POPG 1:1 vesicles were, respectively, at 627 ± 59 μM and 2703 ± 233 μM of phospholipid (POPC vesicles induced no change). The conformational conversion of pep14-23 from random coil to α-helix is thus 4.3-fold lower when interacting with POPG:POPC 1:1 than with vesicles composed of pure POPG (see Supporting Information Table S1) and does not occur in the presence of vesicles composed only of POPC, even at lipid concentrations up to 10 mM. The data shows that electrostatic forces play a significant role in the positively charged pep14-23 (net charge +5) interaction with negatively charged POPG vesicles. This supports the role of anionic phospholipids in pep14-23 (and DENV C N-terminal region) interaction with lipid systems, including the negatively charged LDs.[18,19]

It was recently established that potassium ions are necessary for DENV C interaction with LDs.[18] Therefore, we evaluated the effects of K^+ and Na^+ in pep14-23 binding to anionic membranes and α-helical conversion. Tensiometry (Supporting Information Figure S2A) and zeta potential (Supporting Information Figure S2B) measurements showed that the peptide interacts both with monolayers and bilayers of POPG in the presence of K^+ ions similarly to what it does in the presence of Na^+ ions. Following previous approaches,[18,27,28] the data were fitted using the equations displayed in Table 1. Briefly, lipid monolayers were tested by tensiometry measurements and LUV were used both in zeta potential and in CD measurements. The statistical comparison of the values obtained with Na^+ versus K^+ buffers was performed through an F-test to compare two possible fits, one assuming a given parameter as being different for the distinct data sets and another assuming that parameter to be equal between data sets. Differences were considered significant if $p < 0.05$. As seen from Table 1, the half-maximal effects show for all techniques that there are no significant differences between the results obtained for each ion. Regarding the tensiometry data, the maximum $\Delta\Pi$ obtained upon pep14-23 interaction is higher in Na^+ than in K^+: 5.67 ± 0.14 and 4.55 ± 0.12 mN m^{-1}, respectively (Supporting Information Figure S2A and Table 1). However, a similar half-maximal effect is observed (4.63 ± 0.34 μM and 4.84 ± 0.45 μM for Na^+ and K^+, respectively), with a difference of only 4.5% between each ion, which is not statistically significant (Table 1). The small differences on $\Delta\Pi_{max}$ observed between Na^+ and K^+-containing buffers may be explained by the difference in ion size, which may affect the packing of the lipid monolayer, as suggested by previous works.[29,30] Regarding zeta potential data, $\Delta\zeta$ values also show no difference between the two cations: 26.5 ± 0.95 mV for Na^+ and 27.4 ± 1.34 mV for K^+ buffer (Table 1 and Supporting Information Figure S2B). The difference in half-maximal effect between ions is also not statistically significant (31.9 ± 3.3 μM and 33.5 ± 4.9 μM for Na^+ and K^+, respectively). These $\Delta\zeta$ values imply an apparent lipid to peptide ratio of 6.3 ± 0.7 in Na^+ and 6.0 ± 0.9 in K^+ at the half-maximal effect. CD studies of pep14-23 secondary structure also show no statistically significant difference for POPG vesicles in Na^+ or K^+-containing buffers, with the apparent lipid to peptide ratio at half-maximal effect being 15.7 ± 1.5 in Na^+ and 13.2 ± 1.2 in K^+. These half-maximal effect values derived from CD data compare very well with those obtained via $\Delta\zeta$ analysis. In addition, the minimum of the ellipticity for both ion conditions is very similar, without any statistically significant difference: $-9.83 \pm 0.22 \times 10^3$ deg cm^2 $dmol^{-1}$ Res^{-1} and $-9.60 \pm 0.21 \times 10^3$ deg cm^2 $dmol^{-1}$ Res^{-1}, for Na^+ and K^+, respectively (Table 1 and Supporting Information Figure S2C). Strictly regarding pep14-23 membrane binding and α-helical conversion properties, sodium and potassium ions seem to be associated with very similar behavior.

pep14-23 Shows an α-Helical NMR Structure. To further confirm the α-helical tendency of pep14-23, we used NMR spectroscopy to determine the structure of pep14-23 in the presence of dodecylphosphocholine (DPC) micelles (Figure 3; statistics details are available in Supporting

dx.doi.org/10.1021/cb500640t | ACS Chem. Biol. XXXX, XXX, XXX−XXX

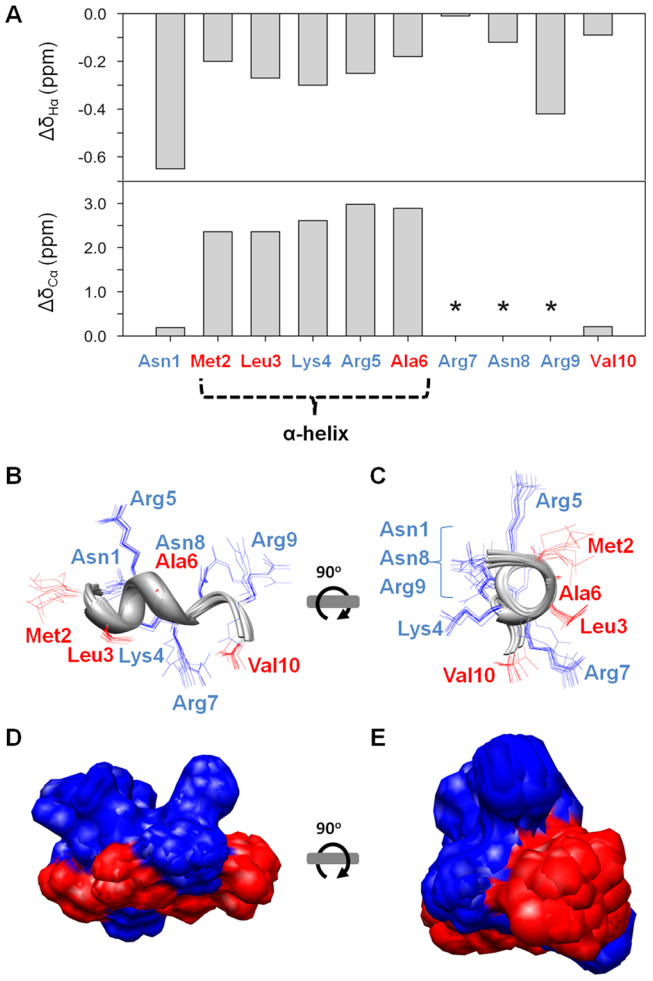

Figure 3. Structure of pep14-23 evaluated by NMR in the presence of DPC micelles. (A) Hα and Cα chemical shift difference ($\Delta\delta = \delta_{measured} - \delta_{random\ coil}$)[32] of pep14-23 residues upon its interaction with DPC micelles. Unassigned chemical shifts are marked with asterisks. Amino acid residues from 2 to 6 correspond to the α-helical segment determined from the consensus between Hα and Cα chemical shift differences and DNANGLE predictions (structure calculation statistics are available in Supporting Information Table S2). Ribbon (B and C) and surface (D and E) representations of the overlay of the 10 lowest energy structures of pep14-23 in the presence of DPC micelles, determined by solution NMR spectroscopy at a DPC to pep14-23 ratio of 200. Hydrophobic side chains are colored red, while hydrophilic side chains are in blue.

Information Table S2). As the corresponding DENV C domain, the peptide is intrinsically disordered in aqueous solution (Figure 2C) but gains structure upon binding to the DPC micelles (Figure 3A), forming an α-helix spanning from Met2 to Ala6. This α-helix has a moderate amphipathic nature (Figure 3B–E), with Met2, Leu3, Ala6, and Val10 at one side of the helix, probably facing the hydrophobic environment of the micelle, and the hydrophilic residues either facing the aqueous environment or with the positively charged residues (Lys4, Arg5, Arg7, and Arg9) establishing Coulombic interaction with the phosphate of the DPC phosphocholine group. The polar residue Arg7 is at the same side of the helix as the hydrophobic residues (Figure 3C), leading to a break in the α-helix at this position (Figure 3B), as it can be noted by the Hα and Cα chemical shift difference ($\Delta\delta_{H\alpha}$ and $\Delta\delta_{C\alpha}$, respectively, Figure 3A). The same was observed from Φ and Ψ dihedrals predicted using the DANGLE software.[31] The negative values of $\Delta\delta_{H\alpha}$ concomitant with positive values of $\Delta\delta_{C\alpha}$ in more than three consecutive residues clearly suggest an α-helical structure,[32] corroborating the CD data (Figure 2C and D, and Supporting Information Figure S2C and D). Interestingly, despite the missing $\Delta\delta_{C\alpha}$, the peptide has a kink in residue Arg7, as suggested by the $\Delta\delta_{H\alpha} \sim 0$ ppm and by the structure calculations (which take into account NOE-derived distance restraints). In spite of this, the α-helical peptide structures still show an amphipathic character with an asymmetric surface charge distribution (Figure 3D–E). The positive charges aligned on one side of the α-helix may facilitate the observed interaction with negatively charged phospholipid model membranes.

DENV C N-Terminus Alternative α-Helical Conformations. It is clear that pep14-23, a proxy for the DENV C N-terminal region, binds negatively charged phospholipids, and converts to α-helical structure independently of Na^+ and K^+ ions. The region of DENV C corresponding to pep14-23 sequence is described as intrinsically disordered in solution.[19,23] This is a major obstacle to experimental structural studies based on NMR or X-ray crystallography, being the reason for the first 20 amino acid residues of DENV being missing from the available NMR structure.[23] To circumvent this problem, the possible tertiary structure(s) that this DENV C region may assume were predicted via I-TASSER (Figure 4).[33] The experimental DENV C NMR structure available (Protein Data Bank (PDB) ID 1R6R[23]), used as a seed template, is shown as ribbon structure in Figure 4A, displaying the homodimer structure formed by residues 21–100. For the N-terminal segment (amino acid residues 1–20), the tertiary structure prediction was made *ab initio*. As expected, the region encompassing residues 21 to 100 has a folding arrangement coincident with the experimental DENV C structure (Figure 4A and gray ribbon structure of Figure 4B). Interestingly, for the N-terminal segment, four feasible possible orientations in the context of the homodimer were obtained. These are represented in Figure 4B (blue, red, yellow, and green ribbon structures; see also Supporting Information Figure S3), superimposed with DENV C experimental homodimer structure (gray ribbon structure). It is clear that this N-terminal segment of DENV C can be in various structural arrangements, which is compatible with the previously reported absence of a unique structure for the N-terminal region.[19,23] It is possible to cluster the generated conformers in two groups: one in which the hydrophobic pocket formed by the $\alpha2$-$\alpha2'$ interface is exposed to the solvent, and the other in which the $\alpha2$-$\alpha2'$ region is shielded by the N-terminal segment (Figure 4B and Supporting Information Figure S3, green- and blue-shadowed conformers, respectively). These alternating closed and open conformations also make sense in terms of the surface charge distribution resulting from the dimer structures formed by such conformers (Supporting Information Figure S3, bottom row). Importantly, the α-helical orientations predicted for the DENV C N-terminal region (Figure 4) are consistent with the postulated α-helical content of the pep14-23 region (Figure 1) and with pep14-23 experimental structural data (Figures 2 and 3). The existence of alternating conformations is also supported by the dynamic and flexible behavior of this region.[19,23,26] Given the limitations in exploring this possibility via experimental methods, to further analyze the stability of the proposed DENV C autoinhibited conformation, a molecular dynamics (MD) simulation on the proposed autoinhibited

dx.doi.org/10.1021/cb500640t | ACS Chem. Biol. XXXX, XXX, XXX–XXX

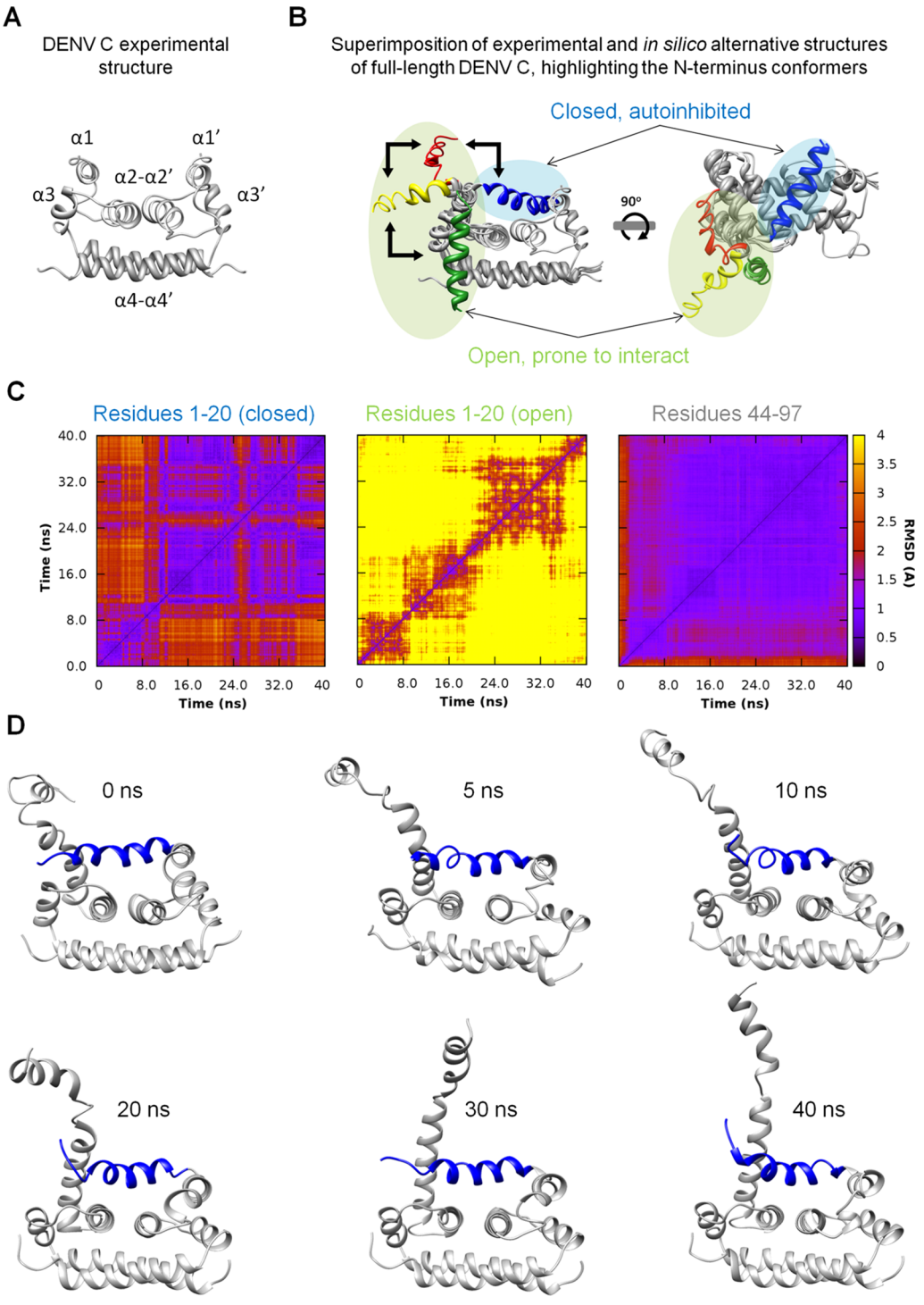

Figure 4. Predicted tertiary structures for DENV C N-terminal region provide insights to protein function. (A) Structure of DENV C (residues 21 to 100) determined by NMR (ribbon view; PDB ID: 1R6R). (B) *In silico* predictions of DENV C tertiary structure showing four possible orientations for the N-terminal disordered region (residues 1−20; different conformations colored blue, red, yellow, and green) that fit into the experimentally determined DENV C homodimer tertiary structure (gray). The blue conformation (blue shadowed area) is shielding the $\alpha 2$-$\alpha 2'$ region and, in this manner, may autoinhibit DENV C interaction with a molecular target. This is in clear contrast with the green shadowed open conformers, where the $\alpha 2$-$\alpha 2'$ region is exposed. (C) RMSD versus time correlation plots obtained from MD simulation (total time 40 ns). The left plot corresponds to residues 1 to 20 in the closed (autoinhibited) DENV C N-terminal conformation. The middle plot corresponds to residues 1 to 20 in the open DENV C N-terminal conformation. The right plot corresponds to residues 44 to 97 of DENV C homodimer (the conserved fold between WNV C and DENV C protein structures[19]). The plot corresponding to residues 21 to 43 is similar to the plot of residues 44−97, being available in Supporting Information Figure S4. The yy axis scale for time is presented on the left side while the RMSD color scale is on the right side. (D) DENV C structure, with N-terminal residues 1−20 in the autoinhibited conformation, colored in blue, at several discrete time points of the MD simulation: 0 (initial structure), 5, 10, 20, 30, and 40 ns. Clearly, residues 1−20 in the closed (autoinhibited) conformation (blue) and residues 44−97 form more stable structures over time, in contrast to residues 1 to 20 belonging to the open conformation.

dx.doi.org/10.1021/cb500640t | *ACS Chem. Biol.* XXXX, XXX, XXX−XXX

structure was performed (Figure 4C−D and Supporting Information Figure S4). These MD simulations allow assessing the stability of the hypothetical conformations. The results indicate stable complexes for both the peptide-bound and the autoinhibited DENV C variants. A starting structure for the autoinhibited conformation was generated by aligning residues 21−100 of the blue model (Figure 4B) with the published NMR structure of DENV C (1R6R[23]). Similarly, the open red model (Figure 4B) was chosen as the starting point for the other half of the C protein. Both were aligned with the complementary chains of the 1R6R dimer to create the starting structure for the full-length autoinhibited DENV C dimer complex. As further detailed in the methods section and Supporting Information, MD simulations were performed for 40 ns using Amber ff14SB interaction potentials at 1.0 bar and 300 K, following standard procedures.[34−36] The results (Figure 4C−D and Supporting Information Figure S4) indicate stable structures for the autoinhibited conformation (Figure 4C, left plot, and Figure 4D, blue colored), with only a small variation occurring through the course of the simulation. There is a variation of RMSD at approximately 10 ns (Figure 4C, left plot), which does not translate in major structural rearrangement of the autoinhibited conformation (Figure 4D, blue colored ribbon structure). This change can be traced to the adaptation of the dimer partner in the contact area to residues 1−20 of the inhibiting monomer. After this adaptation is complete, a stable conformational space is sampled by the complex until the end of the simulation. These structural models thus represent plausible variants for the autoinhibited DENV C dimer conformation (which is thus a possible transient structure for DENV C N-terminal region). Overall, the α-helical structure is maintained, in agreement with the literature data and the experimental findings reported here. As such, it is likely that the DENV C N-terminal region may adopt an α-helical structure, as observed for pep14-23. Moreover, a swift conformational switch (such as the gain of α-helical structure) is behind the physiological role of many similar intrinsically disordered proteins,[24,37] as discussed ahead.

Given all the above, pep14-23 may adopt a similar α-helical structure and interact directly with DENV C hydrophobic pocket. To evaluate this hypothesis, computational studies were performed (Supporting Information Figure S5). A starting structure for the DENV C-pep14-23 complex was obtained by using an open model of the full-length DENV C dimer (as displayed in Supporting Information Figure S3) and the pep14-23 α-helical NMR conformation (shown in Figure 3B−E). The Rosetta protein−protein docking package[38] was employed for docking the peptide onto the protein. The conformations with best interaction scores were chosen as a starting point for MD simulations of DENV C-peptide complex stability. These simulations indicate the formation of a stable complex, as seen from the analysis of two-dimensional RMSD plots (Supporting Information Figure S5A-B). Furthermore, pep14-23 docks into the hydrophobic pocket (Supporting Information Figure S5C), within the same conformational space that the DENV C N-terminal homologous region is expected to occupy. Complementing this, NMR experiments for DENV C interaction with pep14-23 (in the absence of phospholipids) were performed (Supporting Information Figure S6). The results show changes in chemical shift as a result of addition of pep14-23, a good indication that DENV C is affected by the peptide. Although many of the residues affected are arginines and lysines, a number of other amino acid residues of the DENV C N-terminal region seem also to be affected, namely, Met15, Leu16 and Lys17. The peptide may therefore interact with several regions of the DENV C protein, including the N-terminal region and the hydrophobic pocket, as suggested by the MD simulations. Importantly, the N-terminal residues affected by the interaction with pep14-23 are within the homologous 14-23 region of DENV C, belonging also to the conserved ^{14}NMLKR^{18} motif (similar to importin α autoinhibitory motif, discussed hereafter).

DENV C and pep14-23 Similarity to Importin α. The highly dynamic behavior of DENV C N-terminal segment may be important in the context of DENV C interaction with LDs, which involves mostly α2 and N-terminal residues.[16,19] pep14-23 was designed based on this information and on an N-terminal motif conserved among mosquito-borne *Flavivirus* C proteins:[19,20] ^{14}NML+R.[18] Going further, structural analogy comparison was used here to discover if a pep14-23 related sequence could be found in other proteins. Searching via BLASTp through the PDB database for domains with the pep14-23 sequence (NMLKRARNRV), the only proteins found within a meaningful E-value threshold were DENV C and human importin α. If we search for the less restrictive conserved motif (^{14}NMLKR^{18}), the only proteins for which a structure has been deposited at PDB are again DENV C and importin α. These similar sequences are found in the N-terminal regions of both proteins. Therefore, understanding importin α activity may give clues to the analogous DENV C and pep14-23 sequences. Importin α is found in eukaryotic cells, and its function involves binding target proteins in the cytosol to carry them into the nucleus.[39,40] The above-mentioned pep14-23 and DENV C N-terminal-like motif (^{46}NMLKRRNV^{53}) of importin α N-terminus serves to inhibit itself when necessary.[39−42] Coincidentally, this importin α N-terminal motif undergoes a conformational change from random coil to α-helical structure upon ligand binding.[39−42] Such a conformational switch has also been described for other intrinsically disordered protein domains,[37,43−46] where structural changes are triggered by the ligand itself or by the ligand microenvironment (e.g., biomembrane location).[44,46] Similarly, DENV C N-terminal region may also switch from mostly unstructured to an ordered conformation, in accordance with other dynamic flexible protein regions (reviewed elsewhere[45]).

Key Findings. The regions proposed to be affected by the alternative conformations and the autoinhibition are the hydrophobic cleft (helices α1 and α2 of both monomers) and the N-terminal domain of DENV C. These are the same regions shown by NMR to be affected when DENV C interacts with lipid droplets.[19] It is not unlikely that DENV C N-terminal domain interacts with anionic LDs surface phospholipids for specific functions, such as acquiring the proper conformation for subsequent binding to LDs, required for successful viral replication,[16] opening the hydrophobic cleft for the binding to perilipin 3, in agreement with previous data.[18,19] This would prevent unspecific or untimely interactions of the hydrophobic cleft, opening up only when required. DENV C binding to RNA, postulated to occur via the positively charged α4-α4′ region,[23] may depend upon the alternation of the N-terminal region between open and closed conformations. These alternate conformations, by originating alosteric movements within the dimer, may also play a role in modulating DENV C-RNA binding. In other conditions, such as within the highly condensed nucleocapsid environment,[13,15] DENV C would need to adopt most compact and reduced dimensions

dx.doi.org/10.1021/cb500640t | *ACS Chem. Biol.* XXXX, XXX, XXX−XXX

(provided by the autoinhibited conformation), namely to successfully bind RNA and be closely packed inside the mature virion structure. Importantly, intrinsically disordered protein domains are a common way for increasing the functional activity of viruses and other organisms.[47−49] These conformational variants would thus provide greater functional diversity to a reduced proteome of three structural and seven nonstructural proteins.

The approach followed may inspire similar strategies to determine the structural function of other intrinsically disordered proteins, difficult to study by other approaches. As suggested by the predictions (Figure 1), pep14-23 binds to anionic phospholipids, acquiring α-helical conformation (Figure 2 and Supporting Information Figure S2). Furthermore, pep14-23 NMR structure reveals a distinct charge distribution in the presence of lipid micelles (Figure 3). *In silico* studies of the DENV C N-terminal region (Figure 4) support a model by which it alternates between different orientations. The DENV C segment comprising residues 14 to 23 contains several important residues involved in the interaction with LDs, namely the NML+R motif.[19] This motif is similar to the importin α autoinhibitory motif, supporting a parallel autoinhibitory role for that DENV C section. As previously shown, pep14-23 has a clear inhibitory effect on DENV C *in vitro*.[19] Here, it is demonstrated that pep14-23 and the DENV C N-terminal α-helical region in which it is based match the autoinhibitory sequence of importin α. This, together with the previous data reported in the literature and the experimental data and MD simulations presented here suggests the occurrence of alternative N-terminal structural arrangements (Supporting Information Figure S3). These alternative conformers would modulate $\alpha2$-$\alpha2'$ interface accessibility, in agreement with our current understanding of DENV C structure−activity relationship, providing a molecular level explanation for the interaction of DENV C N-terminus and $\alpha2$-$\alpha2'$ interface with LDs and very low-density lipoproteins.[18,19,21] pep14-23, which is based on the DENV C N-terminal region involved in the interaction with LDs,[19] may outcompete the homologous region of the viral protein. The data advance the understanding of DENV C function and sustain the use of peptides based on the capsid protein N-terminal region, with different α-helical propensities, as inhibitory drug leads. This promising avenue of research yielded excellent results in the past, since different peptides and peptide analogues are effective against other viruses, such as HIV and hepatitis C virus.[31,50−52] To conclude, given the similarity between mosquito-borne flaviviruses capsid proteins,[19] the information gathered may lead to future drug development strategies targeting related flaviviruses.

METHODS

Computational Methods. As detailed in the Supporting Information, ProtScale (http://web.expasy.org/protscale/), I-TASSER (http://zhanglab.ccmb.med.umich.edu/I-TASSER), and BLASTp (http://blast.ncbi.nlm.nih.gov/) Web servers were employed for, respectively, hydrophobicity and α-helical propensity predictions, tertiary structure prediction and, finally, sequence similarity search. To further validate the stability of the proposed autoinhibited conformation of DENV C, MD simulations were performed as fully detailed in the Methods section of the Supporting Information.

Chemicals. The peptide pep14-23 (H-NMLKRARNRV-NH_2), rationally designed by us and protected under a patent Nr WO/2012/159187,[20] was custom synthesized by JPT Technologies GmbH (Berlin, Germany) and Schafer-N (Copenhagen, Denmark), with >95% purity, as confirmed by reverse-phase HPLC and ESI-MS analysis. No difference was observed between different batches of peptide or from different suppliers. POPC and POPG were obtained from Avanti Polar Lipids (Alabaster, AL, U.S.A.), and DPC from Cambridge Isotopes (Tewksbury, MA, U.S.A.). Unless otherwise stated, all other chemicals and reagents were purchased from Sigma-Aldrich (St. Louis, MO, U.S.A.). The buffers used in all experiments contained 50 mM NaH_2PO_4 pH 7.4, with 100 mM NaCl (Na^+ buffer) or the same concentration of KCl (K^+ buffer). LUV of phospholipids were prepared by extrusion methods, as described in full detail in the Supporting Information.

Tensiometry. Changes on the surface pressure of pure POPG lipid monolayers induced by pep14-23 were measured on a Nima Langmuir−Blodgett trough ST900 (Coventry, U.K.), at constant temperature (25 ± 0.5 °C). A solution of POPG in chloroform was spread on the surface of Na^+ or K^+ buffer contained within a Teflon recipient of a fixed surface area, until a stable surface pressure of 25.5 ± 0.5 mN m^{-1} was reached, after solvent evaporation. Peptide solutions were injected into the subphase and the variations on the surface pressure of the lipid monolayer were followed during the time necessary to reach a constant value. The initial 25.5 ± 0.5 mN m^{-1} surface pressure was chosen in order to be above the surface pressure of the air−water interface upon injecting the largest peptide concentration in the absence of lipid (15 mN m^{-1}). This ensures that changes in the lipid monolayer surface pressure after peptide injection are only due to the peptide action. All conditions were assessed independently and in triplicate.

Zeta Potential. Zeta potential (ζ) measurements were carried out on a Malvern Zetasizer Nano ZS device following established procedures,[18,19,53] fully detailed in the Supporting Information.

Circular Dichroism Spectroscopy. CD measurements were carried out in a JASCO spectropolarimeter J-815 (Tokyo, Japan), using cuvettes of 1.0 mm path length. Spectra were acquired between 195 and 260 nm, at 25.0 °C, with data pitch of 0.2 nm, wavelength sampling velocity of 200 nm min^{-1}, data integration time of 1 s, and performing at least 3 accumulations. Measurements were conducted both in Na^+ and K^+ buffers, with different lipid concentrations up to 10 mM, with and without 40 μM of pep14-23. In addition to blank subtraction, experimental instrument-related baseline drift was corrected by subtracting to all spectra the average of the signal between 250 and 260 nm. Spectra were normalized to mean residue molar ellipticity (deg cm^2 $dmol^{-1}$ Res^{-1}). For the data fits, $[\theta]_0$ values (pep14-23 signal in the absence of lipid) were not significantly different from -1×10^3 deg cm^2 $dmol^{-1}$ Res^{-1} and were thus set equal to this value in all fits. All conditions were measured independently and in triplicate.

NMR Spectroscopy. As lipid vesicles would be too large for classical nuclear magnetic resonance studies, we employed dodecylphophocholine micelles instead, following previous approaches, as detailed in the Supporting Information.

ASSOCIATED CONTENT

Supporting Information

Experimental details and supplementary figures and tables not required for the understanding of the main manuscript. This material is available free of charge via the Internet at http://pubs.acs.org.

AUTHOR INFORMATION

Corresponding Authors

*Tel.: +351217999480. Fax: +351217999477. E-mail: nsantos@fm.ul.pt.

*Tel.: +351217999476. Fax: +351217999477. E-mail: ivomartins@fm.ul.pt.

Notes

The authors declare no competing financial interest.

■ ACKNOWLEDGMENTS

The authors thank T. Freitas (IMM, FMUL) for technical assistance. This work was supported by Fundação para a Ciência e Tecnologia—Ministério da Educação e Ciência (FCT-MEC, Portugal) projects PTDC/QUI-BIQ/112929/2009 and PTDC/SAU-ENB/117013/2010, Calouste Gulbenkian Foundation (FCG, Portugal) project Science Frontiers Research Prize 2010, European Union project FP7-IRSES MEMPEPACROSS, Conselho Nacional de Desenvolvimento Científico e Tecnológico (CNPq, Brazil, grant numbers 471239/2012-7 and 306669/2013-7) and Fundação Carlos Chagas Filho de Amparo à Pesquisa do Estado do Rio de Janeiro (FAPERJ, Brazil, grant numbers E-26/102.919/2011 and E-26/110.636/2012). A.F.F. and A.H. also acknowledge FCT-MEC fellowships SFRH/BD/77609/2011 and SFRH/BPD/72037/2010, respectively. I.C.M. acknowledges consecutive funding from the FCT-MEC fellowship SFRH/BPD/74287/2010 and the Program "Investigador FCT" (IF/00772/2013 Research Contract).

■ REFERENCES

(1) Bhatt, S., Gething, P. W., Brady, O. J., Messina, J. P., Farlow, A. W., Moyes, C. L., Drake, J. M., Brownstein, J. S., Hoen, A. G., Sankoh, O., Myers, M. F., George, D. B., Jaenisch, T., Wint, G. R., Simmons, C. P., Scott, T. W., Farrar, J. J., and Hay, S. I. (2013) The global distribution and burden of dengue. *Nature 496*, 504−507.

(2) Guzman, M. G., Halstead, S. B., Artsob, H., Buchy, P., Farrar, J., Gubler, D. J., Hunsperger, E., Kroeger, A., Margolis, H. S., Martinez, E., Nathan, M. B., Pelegrino, J. L., Simmons, C., Yoksan, S., and Peeling, R. W. (2010) Dengue: A continuing global threat. *Nat. Rev. Microbiol. 8*, S7−16.

(3) Calisher, C. H., and Gould, E. A. (2003) Taxonomy of the virus family Flaviviridae. *Adv. Virus Res. 59*, 1−19.

(4) Grard, G., Moureau, G., Charrel, R. N., Holmes, E. C., Gould, E. A., and de Lamballerie, X. (2010) Genomics and evolution of Aedes-borne flaviviruses. *J. Gen. Virol. 91*, 87−94.

(5) Enserink, M. (2008) Entomology. A mosquito goes global. *Science 320*, 864−866.

(6) Knowlton, K., Solomon, G., and Rotkin-Ellman, M. (July 2009) *Mosquito-Borne Dengue Fever Threat Spreading in the Americas*, pp 1−16, Natural Resources Defense Council Publications Department, Washington, DC.

(7) Enserink, M. (2010) Infectious diseases. Yellow fever mosquito shows up in Northern Europe. *Science 329*, 736.

(8) Reiter, P. (2010) Yellow fever and dengue: A threat to Europe? *Euro Surveill. 15*, 19509.

(9) La Ruche, G., Souares, Y., Armengaud, A., Peloux-Petiot, F., Delaunay, P., Despres, P., Lenglet, A., Jourdain, F., Leparc-Goffart, I., Charlet, F., Ollier, L., Mantey, K., Mollet, T., Fournier, J. P., Torrents, R., Leitmeyer, K., Hilairet, P., Zeller, H., Van Bortel, W., Dejour-Salamanca, D., Grandadam, M., and Gastellu-Etchegorry, M. (2010) First two autochthonous dengue virus infections in metropolitan France, September 2010. *Euro Surveill. 15*, 19676.

(10) Gjenero-Margan, I., Aleraj, B., Krajcar, D., Lesnikar, V., Klobucar, A., Pem-Novosel, I., Kurecic-Filipovic, S., Komparak, S., Martic, R., Duricic, S., Betica-Radic, L., Okmadzic, J., Vilibic-Cavlek, T., Babic-Erceg, A., Turkovic, B., Avsic-Zupanc, T., Radic, I., Ljubic, M., Sarac, K., Benic, N., and Mlinaric-Galinovic, G. (2011) Autochthonous dengue fever in Croatia, August-September 2010. *Euro Surveill. 16*, 19805.

(11) Alves, M. J., Fernandes, P. L., Amaro, F., Osorio, H., Luz, T., Parreira, P., Andrade, G., Ze-Ze, L., and Zeller, H. (2013) Clinical presentation and laboratory findings for the first autochthonous cases of dengue fever in Madeira island, Portugal, October 2012. *Euro Surveill. 18*, 20398.

(12) Capeding, M. R., Tran, N. H., Hadinegoro, S. R., Ismail, H. I., Chotpitayasunondh, T., Chua, M. N., Luong, C. Q., Rusmil, K., Wirawan, D. N., Nallusamy, R., Pitisuttithum, P., Thisyakorn, U., Yoon, I. K., van der Vliet, D., Langevin, E., Laot, T., Hutagalung, Y., Frago, C., Boaz, M., Wartel, T. A., Tornieporth, N. G., Saville, M., and Bouckenooghe, A. (2014) Clinical efficacy and safety of a novel tetravalent dengue vaccine in healthy children in Asia: a phase 3, randomised, observer-masked, placebo-controlled trial. *Lancet 384*, 1358−1365.

(13) Mukhopadhyay, S., Kuhn, R. J., and Rossmann, M. G. (2005) A structural perspective of the flavivirus life cycle. *Nat. Rev. Microbiol. 3*, 13−22.

(14) Urcuqui-Inchima, S., Patino, C., Torres, S., Haenni, A. L., and Diaz, F. J. (2010) Recent developments in understanding dengue virus replication. *Adv. Virus Res. 77*, 1−39.

(15) Kuhn, R. J., Zhang, W., Rossmann, M. G., Pletnev, S. V., Corver, J., Lenches, E., Jones, C. T., Mukhopadhyay, S., Chipman, P. R., Strauss, E. G., Baker, T. S., and Strauss, J. H. (2002) Structure of dengue virus: implications for flavivirus organization, maturation, and fusion. *Cell 108*, 717−725.

(16) Samsa, M. M., Mondotte, J. A., Iglesias, N. G., Assuncao-Miranda, I., Barbosa-Lima, G., Da Poian, A. T., Bozza, P. T., and Gamarnik, A. V. (2009) Dengue virus capsid protein usurps lipid droplets for viral particle formation. *PLoS Pathog. 5*, e1000632.

(17) Boulant, S., Targett-Adams, P., and McLauchlan, J. (2007) Disrupting the association of hepatitis C virus core protein with lipid droplets correlates with a loss in production of infectious virus. *J. Gen. Virol. 88*, 2204−2213.

(18) Carvalho, F. A., Carneiro, F. A., Martins, I. C., Assuncao-Miranda, I., Faustino, A. F., Pereira, R. M., Bozza, P. T., Castanho, M. A. R. B., Mohana-Borges, R., Da Poian, A. T., and Santos, N. C. (2012) Dengue virus capsid protein binding to hepatic lipid droplets is K +-dependent and mediated by droplets surface proteins. *J. Virol. 86*, 2096−2108.

(19) Martins, I. C., Gomes-Neto, F., Faustino, A. F., Carvalho, F. A., Carneiro, F. A., Bozza, P. T., Castanho, M. A. R. B., Mohana-Borges, R., Almeida, F. C. L., Santos, N. C., and Da Poian, A. T. (2012) The disordered N-terminal region of dengue virus capsid protein contains a drug targetable lipid droplet-binding motif. *Biochem. J. 444*, 405−415.

(20) Martins, I. C., Almeida, F. C. L., Santos, N. C., Da Poian, A. T. (2012) *DENV-Derived Peptides and Methods for the Inhibition of the Flavivirus Replication*; Universidade Federal do Rio de Janeiro (UFRJ), Universidade de Lisboa (UL), Instituto de Medicina Molecular (IMM). International Patent Publication Nr WO/2012/159187.

(21) Faustino, A. F., Carvalho, F. A., Martins, I. C., Castanho, M. A. R. B., Mohana-Borges, R., Almeida, F. C. L., Da Poian, A. T., and Santos, N. C. (2014) Dengue virus capsid protein interacts specifically with very low-density lipoproteins. *Nanomedicine: NBM 10*, 247−255.

(22) Hickenbottom, S. J., Kimmel, A. R., Londos, C., and Hurley, J. H. (2004) Structure of a lipid droplet protein; the PAT family member TIP47. *Structure 12*, 1199−1207.

(23) Ma, L., Jones, C. T., Groesch, T. D., Kuhn, R. J., and Post, C. B. (2004) Solution structure of dengue virus capsid protein reveals another fold. *Proc. Natl. Acad. Sci. U. S. A. 101*, 3414−3419.

(24) Henzler-Wildman, K., and Kern, D. (2007) Dynamic personalities of proteins. *Nature 450*, 964−972.

(25) White, S. H., and Wimley, W. C. (1999) Membrane protein folding and stability: physical principles. *Annu. Rev. Biophys. Biomol. Struct. 28*, 319−365.

(26) Jones, C. T., Ma, L., Burgner, J. W., Groesch, T. D., Post, C. B., and Kuhn, R. J. (2003) Flavivirus capsid is a dimeric alpha-helical protein. *J. Virol. 77*, 7143−7149.

(27) Greenfield, N. J. (2006) Determination of the folding of proteins as a function of denaturants, osmolytes or ligands using circular dichroism. *Nat. Protoc. 1*, 2733−2741.

(28) Sanchez-Martin, M. J., Cruz, A., Busquets, M. A., Haro, I., Alsina, M. A., and Pujol, M. (2012) Physicochemical characterization of GBV-C E1 peptides as potential inhibitors of HIV-1 fusion peptide: interaction with model membranes. *Int. J. Pharm. 436*, 593−601.

(29) Yang, H., Xu, Y., Gao, Z., Mao, Y., Du, Y., and Jiang, H. (2010) Effects of Na+, K+, and Ca2+ on the structures of anionic lipid bilayers and biological implication. *J. Phys. Chem. B 114*, 16978−16988.
(30) Redondo-Morata, L., Oncins, G., and Sanz, F. (2012) Force spectroscopy reveals the effect of different ions in the nanomechanical behavior of phospholipid model membranes: the case of potassium cation. *Biophys. J. 102*, 66−74.
(31) Cheung, M. S., Maguire, M. L., Stevens, T. J., and Broadhurst, R. W. (2010) DANGLE: A Bayesian inferential method for predicting protein backbone dihedral angles and secondary structure. *J. Magn. Reson. 202*, 223−233.
(32) Wishart, D. S., Sykes, B. D., and Richards, F. M. (1992) The chemical shift index: a fast and simple method for the assignment of protein secondary structure through NMR spectroscopy. *Biochemistry 31*, 1647−1651.
(33) Roy, A., Kucukural, A., and Zhang, Y. (2010) I-TASSER: a unified platform for automated protein structure and function prediction. *Nat. Protoc. 5*, 725−738.
(34) Case, D. A., Babin, V., Berryman, J. T., Betz, R. M., Cai, Q., Cerutti, D. S., Cheatham, T. E., III, Darden, T. A., Duke, R. E., Gohlke, H., Goetz, A. W., Gusarov, S., Homeyer, N., Janowski, P., Kaus, J., Kolossváry, A., Kovalenko, T. S., Lee, T. S., LeGrand, S., Luchko, T., Luo, R., Madej, B., Merz, K. M., Paesani, F., Roe, D. R., Roitberg, A., Sagui, C., Salomon-Ferrer, R., Seabra, G., Simmerling, C. L., Smith, W., Swails, J., Walker, R. C., Jang, J., Wolf, R. M., Wu, X., and Kollman, P. A. (2014) AMBER14, University of California, San Francisco.
(35) Berendsen, H. J. C., Postma, J. P. M., Vangunsteren, W. F., Dinola, A., and Haak, J. R. (1984) Molecular-Dynamics with Coupling to an External Bath. *J. Chem. Phys. 81*, 3684−3690.
(36) Loncharich, R. J., Brooks, B. R., and Pastor, R. W. (1992) Langevin dynamics of peptides: the frictional dependence of isomerization rates of N-acetylalanyl-N′-methylamide. *Biopolymers 32*, 523−535.
(37) Fermani, S., Trivelli, X., Sparla, F., Thumiger, A., Calvaresi, M., Marri, L., Falini, G., Zerbetto, F., and Trost, P. (2012) Conformational selection and folding-upon-binding of intrinsically disordered protein CP12 regulate photosynthetic enzymes assembly. *J. Biol. Chem. 287*, 21372−21383.
(38) Gray, J. J., Moughon, S., Wang, C., Schueler-Furman, O., Kuhlman, B., Rohl, C. A., and Baker, D. (2003) Protein-protein docking with simultaneous optimization of rigid-body displacement and side-chain conformations. *J. Mol. Biol. 331*, 281−299.
(39) Lange, A., Mills, R. E., Lange, C. J., Stewart, M., Devine, S. E., and Corbett, A. H. (2007) Classical nuclear localization signals: definition, function, and interaction with importin α. *J. Biol. Chem. 282*, 5101−5105.
(40) Catimel, B., Teh, T., Fontes, M. R., Jennings, I. G., Jans, D. A., Howlett, G. J., Nice, E. C., and Kobe, B. (2001) Biophysical characterization of interactions involving importin-α during nuclear import. *J. Biol. Chem. 276*, 34189−34198.
(41) Kobe, B. (1999) Autoinhibition by an internal nuclear localization signal revealed by the crystal structure of mammalian importin α. *Nat. Struct. Biol. 6*, 388−397.
(42) Fontes, M. R., Teh, T., and Kobe, B. (2000) Structural basis of recognition of monopartite and bipartite nuclear localization sequences by mammalian importin-α. *J. Mol. Biol. 297*, 1183−1194.
(43) Moritsugu, K., Terada, T., and Kidera, A. (2012) Disorder-to-order transition of an intrinsically disordered region of sortase revealed by multiscale enhanced sampling. *J. Am. Chem. Soc. 134*, 7094−7101.
(44) Popovic, M., De Biasio, A., Pintar, A., and Pongor, S. (2007) The intracellular region of the Notch ligand Jagged-1 gains partial structure upon binding to synthetic membranes. *FEBS J. 274*, 5325−5336.
(45) Kobe, B., and Kemp, B. E. (1999) Active site-directed protein regulation. *Nature 402*, 373−376.
(46) Barre, P., and Eliezer, D. (2006) Folding of the repeat domain of tau upon binding to lipid surfaces. *J. Mol. Biol. 362*, 312−326.
(47) Peng, Z., Yan, J., Fan, X., Mizianty, M. J., Xue, B., Wang, K., Hu, G., Uversky, V. N., Kurgan, L. (2014) Exceptionally abundant exceptions: comprehensive characterization of intrinsic disorder in all domains of life, *Cell. Mol. Life Sci.* Epub Jun 18, 2014. DOI: 10.1007/s00018-014-1661-9.
(48) Darlix, J. L., de Rocquigny, H., Mauffret, O., Mely, Y. (2014) Retrospective on the all-in-one retroviral nucleocapsid protein, *Virus Res.* Epub Jun 4, 2014. DOI: 10.1016/j.virusres.2014.05.011.
(49) Fan, X., Xue, B., Dolan, P. T., LaCount, D. J., Kurgan, L., and Uversky, V. N. (2014) The intrinsic disorder status of the human hepatitis C virus proteome. *Mol. Biosyst. 10*, 1345−1363.
(50) Szoka, F., Olson, F., Heath, T., Vail, W., Mayhew, E., and Papahadjopoulos, D. (1980) Preparation of unilamellar liposomes of intermediate size (0.1−0.2 μmol) by a combination of reverse phase evaporation and extrusion through polycarbonate membranes. *Biochim. Biophys. Acta 601*, 559−571.
(51) Tulumello, D. V., and Deber, C. M. (2009) SDS micelles as a membrane-mimetic environment for transmembrane segments. *Biochemistry 48*, 12096−12103.
(52) Seddon, A. M., Curnow, P., and Booth, P. J. (2004) Membrane proteins, lipids and detergents: not just a soap opera. *Biochim. Biophys. Acta 1666*, 105−117.
(53) Domingues, M. M., Inacio, R. G., Raimundo, J. M., Martins, M., Castanho, M. A. R. B., and Santos, N. C. (2012) Biophysical characterization of polymyxin B interaction with LPS aggregates and membrane model systems. *Biopolymers 98*, 338−344.